JCTC Journal of Chemical Theory and Computation

Article

pubs.acs.org/JCTC

Hydration of Cisplatin Studied by an Effective *Ab Initio* Pair Potential Including Solute−Solvent Polarization

Andrea Melchior,[†,‡] José Manuel Martínez,[‡] Rafael R. Pappalardo,[‡] and Enrique Sánchez Marcos*[,‡]

[†]University of Udine, Department of Environmental and Physical Chemistry, 33100 Udine, Italy

[‡]University of Seville, Department of Physical Chemistry, 41012 Seville, Spain

Supporting Information

ABSTRACT: The hydration of cis-$[PtCl_2(NH_3)_2]$ (cisplatin) has been studied by means of classical molecular dynamics simulations using a new interaction potential obtained by fitting about 4000 *ab initio* interaction energies calculated at the MP2 level. The functional form included several r^{-n} terms (n = 4, 6, 8, 12) to achieve an accurate description of the interactions in the different regions around the cisplatin. Bulk solvent effects on the cisplatin−water molecule interactions have been included by means of a continuum model. Radial Distribution Function (RDF) analysis does not provide a clear enough description of the hydration pattern due to the intricate solvent arrangement around the solute. Angle-solved RDFs and spatial distribution functions have been used to provide more detailed pictures of the local hydration structure around the two ligands, chloride and ammine groups, and the axial region. Based on this information, it is shown a more convenient way to compute the running coordination number for the first hydration shell by simultaneously considering angle-solved RDFs centered on the ligand representative atoms of the complex: ammino N, Cl, and Pt atoms. This way, the hydration number is obtained by integrating over an interlocking-sphere volume built by the spheres centered on the cation and the main atoms of each ligand. Compared to previous works dealing with cisplatin hydration, the global hydration number for the first coordination shell is now higher and involves about 27 water molecules. The importance of the structural sampling, the computational level, as well as the functional form adopted for the interaction potential are thoroughly discussed with respect to the previous proposed intermolecular potential.

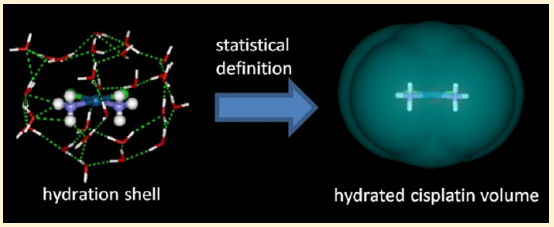

1. INTRODUCTION

Platinum-based drugs are involved in many chemotherapy treatments of a variety of malignancies. In particular, cisplatin has long been employed for a large number of tumors.[1] The accepted action mechanism of cisplatin is based on two stages: the first one is an intracellular activation by the hydrolysis of one chloride ligand, and the second one is the formation of intrastrand cross-links in DNA through the covalent binding of the Pt complex to purine bases. The result is a bent DNA that causes the cell death.[2] Despite the vast number of studies on antitumor drugs based on square-planar platinum complexes, the mechanisms of action and deactivation still need further understanding. It is known that, for cisplatin and its derivatives, the hydrolysis with the chloride ligand release is the rate-determining-step of the process leading to the coordination to DNA.[3−7] For this reason, these reactions have been the subject of a large number of quantum-mechanical studies aimed at correlating molecular factors to the observed kinetic parameters.[8−19] Most of these studies employed continuum solvent models in calculations, but some of them[11,17,18] evidenced the crucial role of explicit solvation on the hydrolysis reaction rates for different platinum-based compounds. Recently, the need for a detailed molecular description of the hydration of platinum-based anticancer drugs stimulated a number of classical Monte Carlo (MC)[20] and molecular dynamics (MD)[21] as well as *ab initio*-MD simulation studies.[17,22] The aim is to obtain a more detailed picture of water structure around cisplatin and its hydrolysis products. These studies belong to the general topic of the square-planar complex hydration, which has attracted growing interest in the past decade, both from an experimental and theoretical point of view. In particular, quantum-mechanics and MD simulations were carried out to study the hydration of the anionic[23−26] $PtCl_4^{2-}$ and cationic $Pt(H_2O)_4^{2+}$ complexes.[27−29] From these studies, peculiar features of the Pt(II) aquaion emerged, such as the axial hydration structure characterized by structural and dynamic properties markedly different from those of the first and the second shells.[28−30] Interestingly, differing from the aquaion case, no axial hydration has been reported for the neutral cisplatin.[20,21] Hydration of Pt(II) square planar complexes in solution has also been subject of experimental studies carried out by means of X-ray absorption (EXAFS)[23,31,32] and ^{195}Pt NMR.[25,26] In such solution studies, *ab initio* MD simulations have been shown to be useful tools in the interpretation of spectroscopic data. However, although *ab initio* MD methods have the advantage of on-the-fly updating of the system wave function, they can only compute short simulation times and a reduced number of water

Received: May 27, 2013

dx.doi.org/10.1021/ct400433c | J. Chem. Theory Comput. XXXX, XXX, XXX−XXX

molecules. This limits the phase space sampling and the physicochemical properties to be examined.

Alternatively, classical MD simulations allow the exploration of much larger time scales, but they need the development of reliable interaction potentials based on *ab initio* and/or experimental data of the system of interest. Classical Lennard-Jones (LJ) interaction potentials to study the hydration of the cis-[20,21] and trans-platin[21] have been recently developed by fitting *ab initio* interaction energies. In these works, Monte Carlo and MD simulations provide insights into the cisplatin hydration, although some differences are observed. For instance, a significantly different number of water molecules in the first solvation shell of platinum complex has been found in these two works, 18.9 (MC)[20] and 12.4 (MD).[21] This disagreement could be due to the different simulation protocols. Density Functional Theory (DFT) calculations[18] on cisplatin hydrated by 15 water molecules suggested that the water molecule number to fully hydrate the complex should be much higher. In those works, the analysis of the axial region has also been somewhat disregarded despite it being an interesting feature of the Pt(II) square-planar complexes.

This study presents results of classical molecular dynamics simulations carried out by using a cisplatin−water interaction potential built by fitting *ab initio* interaction energies of a large number of cisplatin−water structures. Differently from previous studies on cisplatin,[20,21] the new *effective* two-body potential has been developed using interaction energies, which include the polarization of the interacting species, that is, the solute and the water molecule, by a polarizable continuum solvent. This strategy, previously employed to describe Ca^{2+} in water,[33] and ammonia−water mixtures,[34] has been used to take into account the polarization effects on water and cisplatin induced by bulk solvent. Then, many-body effects can be implicitly included in the solute−solvent potential.

2. METHODS

2.1. Potential Development. Quantum-mechanical calculations were carried out at the second-order Møller−Plesset perturbation theory level (MP2). Kozelka and colleagues[16,35] have shown the good behavior of this computational level to deal with the cisplatin−water interaction. Platinum atom was described by means of the Stuttgart−Dresden pseudopotential,[36] whereas for the rest of the atoms 6-31+G(d,p) basis sets were employed. Two-body interaction energies were calculated using the SPC/E geometry[37] for water molecules.

The new two-body cisplatin−water interaction potential (hereafter, "cisPt-W") has been developed in the presence of a polarizable dielectric continuum that models the rest of the solvent as an isotropic medium surrounding the dimer (cisplatin and a water molecule). The electrostatic potential generated by the solute charge distribution induces a polarization charge σ on the molecular-shaped cavity surface because of solvent polarization.[38] This also induces a solute charge redistribution that is taken into account in the Hamiltonian:

$$\hat{H} = \hat{H}^{(0)} + \hat{V}_\sigma \tag{1}$$

where $\hat{H}^{(0)}$ is the gas-phase Hamiltonian (whose eigenfunctions can be denoted as $\Psi^{(0)}$) and $\hat{V}_\sigma$ is the one-electron operator collecting the electrostatic interaction associated to the potential generated by the charge distribution σ present on the surface of a cavity that contains the solute. If two generic fragments A and B are considered, the two-body interaction energy U_{AB} can be defined as[39]

$$U_{AB} = \langle\Psi|\hat{H}^{(0)}|\Psi\rangle_{AB} - \langle\Psi|\hat{H}^{(0)}|\Psi\rangle_{A} - \langle\Psi|\hat{H}^{(0)}|\Psi\rangle_{B} \tag{2}$$

where Ψ are eigenfunctions of the $\hat{H}$ operator (1) corresponding to the complex AB and to the isolated fragments embedded in the solvent. Equation 2 provides a definition for U_{AB} where the interaction energies of A, B, and AB with the dielectric continuum have been removed, yielding only the direct interaction in vacuum between A and B, but with their wave functions polarized by the dielectric medium. During the MD computer simulations, the solute-continuum interaction is replaced by explicit polarized solvent molecules that interact with the polarized solute fragments according to their specific interaction potentials. It is worth noting at this point that if one had used $\hat{H}$ of eq 1 to compute U_{AB} in eq 2, the solute−solvent interactions would have been calculated twice when computer simulations were carried out.

When building *ab initio* based interaction potentials, the use of a large number of solute−solvent arrangements obtained through a Potential Energy Surface scan process is common. The fact that the interaction energy is affected by the Basis Set Superposition Error (BSSE) when finite basis sets are employed for the quantum mechanical description of the fragments is well known. In this particular case, this affects not only the absolute value of the interaction energy but also the even-tempered potential, as BSSE depends on distance. This is the reason why the counterpoise method (CP)[40] has been employed to estimate this deficiency. However, it is generally accepted that the full CP correction overestimates the BSSE, its magnitude being largely dependent on the basis sets and method employed, as recently carefully reconsidered.[41,42] For MP2 interaction energies based on relatively modest basis sets, Kim and colleagues suggest the application of only 50% of the CP correction.[43] To check the suitability of this procedure to our computation level, the BSSE estimation with a series of basis sets of increasing quality has been computed for one of the scan used in the potential building. Figure S1 in the Supporting Information (SI) shows the interaction energy, E_{int}, corresponding to an attractive approaching of a water molecule to the cisplatin unit, following the arrangement shown in the same figure, which, in fact, contains one structure close to the absolute minimum. Together with the basis sets employed in the potential development (6-31+G(d,p)), results obtained with the larger aug-cc-pvTZ and aug-cc-pvQZ basis sets have also been included. For each basis sets, interaction energies with 100% of CP correction, 50% or without correction are plotted. The *ab initio* interaction energy BSSE corrected by means of the CP method is computed according to the following expression

$$\begin{aligned} E_{int} &= U_{AB} + a\Delta E^{CP} \\ &= U_{AB} + a[(E_A - E_A^{CP}) + (E_B - E_B^{CP})] \end{aligned} \tag{3}$$

where the CP correction is weighted by factor a, which in our case, takes the value 0 (no correction), 0.5 (50%), or 1 (100%), and fragment energies, E_i, correspond to gas phase computations. Table 1 collects E_{int} corresponding to the minima of the different curves, in order to provide a quantitative idea on the relative importance of the BSSE correction.

dx.doi.org/10.1021/ct400433c | J. Chem. Theory Comput. XXXX, XXX, XXX−XXX

Table 1. Interaction Energy (kcal/mol) of the Minimum Energy Structure Corresponding to the Approaching Cisplatin−Water Curve Plotted in Figure S1 (SI)

	E_{int}(kcal/mol)		
basis sets	without BSSE	50%-BSSE	100%-BSSE
6-31+G(d,p)	−15.0	−13.3	−11.6
aug-cc-pvTZ	−14.9	−14.0	−13.1
aug-cc-pvQZ	−14.1	−13.7	−13.3

In all cases, larger BSSE corrections are found near the minima (range 3.0−3.5 Å) and in the repulsive region, decreasing steeply and asymptotically as distance increases. The largest correction (E_{int}(100%) − E_{int}(without)), appears for the smallest basis sets, 6-31+G(d,p), (3.4 kcal/mol) whereas the largest aug-cc-pvQZ ones presents the smallest correction, (0.8 kcal/mol). Thus, the non-BSSE corrected E_{int} curve is conversely more attractive for the smallest basis sets (−15.0 kcal/mol) than for the largest ones (−14.1 kcal/mol). As claimed by several authors, the optimal performance provided by very large basis sets would lead to negligible BSSE, and there would not need of any kind of BSSE correction.[41,42,44] This is clearly observed in Figure S1, and quantitatively shown in Table 1. E_{int} results show that a 50% CP correction (−13.3 kcal/mol) is quite reasonable for the basis sets here used, if compared with the larger aug-cc-pvQZ ones. As expected, intermediate basis sets, such as the aug-cc-pvTZ ones (−14.0 kcal/mol), may provide improved curves, when applying a 50% CP correction, but the computational cost increases as much as a 100 times, and increases up to 1400 times if aug-cc-pvQZ is considered. These increases would have prevented the exhaustive prospection of the Potential Energy Surface carried out with the 6-31+G(d,p) basis sets and consequently would have led to a less detailed description of the cisplatin−water interaction.

All calculations were performed with the Gaussian09 program.[45]

The functional form of the interaction potential used to fit the BSSE-corrected cisplatin−water *ab initio* interaction energies was

$$V(r_{ij}) = \sum_{i}^{\text{cisplatin sites}} \sum_{j}^{\text{water sites}} \frac{C_{ij}^{4}}{r_{ij}^{4}} + \frac{C_{ij}^{6}}{r_{ij}^{6}} + \frac{C_{ij}^{8}}{r_{ij}^{8}} + \frac{C_{ij}^{12}}{r_{ij}^{12}} + \frac{q_i q_j}{r_{ij}} \quad (4)$$

A total of 3923 interaction energies were used to fit the parameters in eq 4. Only structures with interaction energies smaller than +20 kcal mol^{-1} were considered for the fitting. The values of the best fit coefficients are reported in Table 2. The electrostatic part of the interaction is defined by charges obtained by fitting the electrostatic potential of the solvent−polarized solute wave function according to the Merz−Singh−Kollman scheme.[46] Partial atomic charges are also given in Table 2.

It is worth pointing out that, during the fitting process, no sign constraints to the 32 fitted coefficients were imposed. Thus, the potential contains a large number of dependencies, which clouds the physical interpretation usually made on the different terms of more simple potentials like the Lennard-Jonnes one. Although it would have been possible to carry out fits constraining the sign of the corresponding parameters, this led to worse fits. This is one of the reasons why a carefully

Table 2. Site−Site Parameters (C_{ij}^{n}) (kcal/mol Å^{n}) and Cisplatin Partial Atomic Charges Used in eq 4 for the cisPt-W Potential

pair interaction				
$i-j$	C_{ij}^{4}	C_{ij}^{6}	C_{ij}^{8}	C_{ij}^{12}
Pt−OW	−3938.58	48147.70	−154913.96	538408.22
Pt−HW	415.70	−1974.88	3741.87	−1547.30
Cl−OW	2440.09	61620.20	405788.96	−3909292.79
Cl−HW	−301.28	5006.15	−15694.87	35735.81
N−OW	1008.10	15129.06	79017.69	−399043.98
N−HW	−557.48	−1274.64	13215.58	−49486.14
H−OW	−222.07	1294.93	−1857.22	1264.05
H−HW	268.16	−885.01	961.47	−363.26
atomic charges q_i (e)				
Pt		Cl	N	H
0.0534		−0.4829	−0.3649	0.2737

check of the interaction potential behavior must be done in order to detect abnormal attractive zones (i.e., potential *holes*) at short distances.

2.2. Molecular Dynamics Simulations. Classical MD simulations were carried out with the DLPOLY program[47] modified in order to include the type of potential given in eq 4. Cisplatin was placed in a cubic box with 1000 SPC/E[37] water molecules. The box side was set to 31.245 Å, to reproduce the density of 0.997 g cm^{-3} at 298.1 K. Periodic boundary conditions were applied. The optimized cisplatin geometry was kept rigid during molecular dynamics simulations.

After an equilibration period of 100 ps, a simulation of 2.0 ns was run in the canonical ensemble (NVT) using a time step of 1 fs. The Nosé−Hoover thermostat, with a time constant of 0.5 ps, was applied to keep the average temperature at 298.15 K. The cutoff for interactions was 13.0 Å, and electrostatic interactions were treated by the smooth particle mesh Ewald sum method.[48] Atomic positions and velocities were saved every 100 steps for analysis. The system stability was also checked by running a test simulation with the temperature set at 373.15 K. This allows us to check that there are not abnormally high attractive regions in the potential that might easily be achieved by the system. For the sake of comparison, a simulation employing the published cisplatin−water LJ potential parameters[20] (hereafter, "Lopes et al.'s potential") for cisplatin with 1000 TIP3P[49] water molecules was carried out under the same simulation conditions of ours.

3. RESULTS AND DISCUSSION

3.1. Development of the Water−Cisplatin Potential. The correlation between the *ab initio* interaction energies (E_{MP2}) and those calculated (E_{pot}) with the cisPt-W potential is displayed in Figure S2a of Supporting Information (SI). The good agreement found is supported by a quite small standard deviation (SD) between calculated and reference energies (σ = 1.6 kcal mol^{-1}). The same set of *ab initio* interaction energies were fitted to a 6−12 (Lennard-Jones) functional form (hereafter, "cisPt-W/LJ"), the standard deviation being σ = 2.1 kcal mol^{-1} (Figure S2b, SI). SD values reduce to 1.1 and 1.4 kcal mol^{-1} for cisPt-W and cisPt-W/LJ, respectively, when only the attractive sample points ($E_{int} \leq 0$) are considered. The comparison of the two distributions shows an improvement in reproducing the MP2 energies when passing from the cisPt-W/LJ to the cisPt-W potential. Although SD difference for both

dx.doi.org/10.1021/ct400433c | J. Chem. Theory Comput. XXXX, XXX, XXX−XXX

fittings could seem small, it has a non-negligible effect on water distribution around the complex, as will be shown. In particular, it should be noted that the configurations with the most attractive energies, that is, the most statistically representative ones, are better reproduced by the cisPt-W potential. The finer performance of the cisPt-W potential is a consequence of its higher flexibility provided by the two additional terms, r^{-4} and r^{-8}. To double-check the reliability of the new potentials, ca. 140 cisplatin−water dimers were randomly extracted from an MD simulation. The MP2 interaction energies for those configurations were compared with the values predicted by the cisPt-W and cisPt-W/LJ potentials, SD values were 1.3 and 2.0 kcal mol^{-1}, respectively.

One of the optimized structures of the cisplatin-H_2O dimer obtained by using the cisPt-W potential is displayed in Figure 1a together with the minimum obtained by Lopes at al.'s

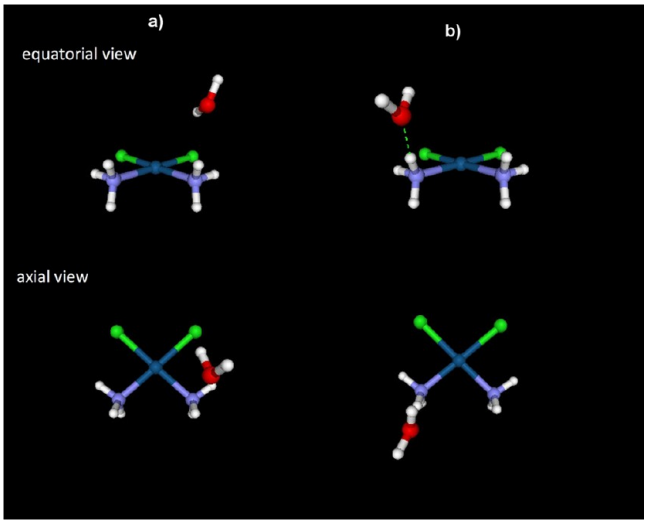

Figure 1. Absolute minima obtained by optimizing the relative positions of cisplatin and water molecule using (a) the cisPt-W potential (E_{int} = −12.6 kcal mol^{-1}), (b) Lopes et al.'s potential[20] (E_{int} = −9.1 kcal mol^{-1}).

potentials (Figure 1b). Their E_{int} values are −12.6 and −9.1 kcal mol^{-1}, respectively. The two structures are rather different since the water molecule is interacting with both ammonia and chloride ligands for the cisPt-W potential (Figure1a), whereas it only interacts with ammonia for Lopes et al.'s potential (Figure 1b). Although the potential development methodology precludes a direct comparison of this minimum with that obtained from the *ab initio* optimized structure, it is worth pointing out that a quite similar structure, which also exhibits a 2-fold hydrogen bond is found by Robertazzi and Platts in a previous quantum-mechanical study on the cisplatin hydration[11] (see Figure 3a in ref 11), using B3LYP and similar basis sets to those here employed. Our quantum-mechanical level predicts a similar optimization structure as well. The global minimum derived from the approaching curve of Figure S1 (SI) is also an optimized structure with E_{int} = −12.7 kcal/mol, exhibiting an arrangement close to that of Lopes et al.'s potential. The fact that the water−cisplatin interaction is stronger with the new potential than with Lopes et al.'s potential can be visualized in a 3D representation of iso-surfaces corresponding to both interaction potentials. Figure 2 plots iso-surfaces for an interaction energy value of −8.5 kcal mol^{-1}. Potentials are mapped on a 10 × 10 × 4 Å^3 box centered on the Pt atom (grid bin of 0.05 Å in each direction). These plots show that the new potential has not only a more attractive character (a more extended space region is plotted despite the lower energy cutoff) but also a rather different topology. Lopes et al.'s potential has quite well located regions close to the ammonia hydrogen atoms, explaining the optimized structure (Figure 1b). For the cisPt-W potential, the distribution is much more widespread in space, covering the regions where the minimum in Figures 2a and S1 are observed.

The origin of the stronger cisplatin−H_2O interaction given by the cisPt-W potential than by Lopes et al.'s one must be understood on the basis of the different methodologies employed in their development, including the solvent effects on the polarization of the solute wave function, the more exhaustive exploration around the cisplatin complex (∼4000 points for the cisPt-W vs 320 points for Lopes et al.'s potential) and the functional form adopted in the fitting. Once analyzed the impact of the new intermolecular potential on the cisplatin hydration, the behavior of the new potential will be rationalized.

3.2. Hydration of Cisplatin: Radial Distribution Functions. Platinum−oxygen (OW) and −hydrogen (HW) radial distribution functions (RDF) calculated in the simulation with the cisPt-W potential are shown in Figure 3a (left), The same pair distributions obtained with the simulation using Lopes et al.'s potential are also plotted (Figure 3a, right).

The cisPt-W Pt−OW RDF presents a wide peak centered at 4.0 Å, which extends up to 6 Å, showing two humps at *ca.* 4.6 and 5.5 Å. They are indicating different contributions to this global peak. The position of the first maximum is in good agreement with the Pt−OW RDF obtained by recent *ab initio* FMO-MD calculations[22] (Table 3). Pt-HW RDF shows a wide asymmetric first peak that also results from several contributions from different ligand regions around the Pt. This peak extends to shorter distances than the corresponding to the Pt-OW pair. A simulation employing Lopes et al.'s potential presents Pt−OW and Pt−HW RDFs quite different from ours; in particular, their first-peak height and width are smaller. The most noticeable difference is the integration of the Pt-OW RDF, which gives a number of water molecules in its first hydration shell, *n*, significantly smaller (12) than those obtained with the cisPt-W potential (28). The Pt-HW RDF provided by simulation using Lopes et al.'s potential gives a less wide and intense first peak that represents a smaller number of hydrogen atoms (23) than that obtained by the cisPt-W potential (57).

Since the axial region of Pt(II) has been shown to present peculiar structural and dynamical features in other planar species,[24,25,27,29,30,50] it is worth examining this region in particular. To this aim, an angular decomposition of the global RDFs has been carried out, using the procedure previously applied to the hydration of Pd(II) and Pt(II) aquaions.[50] The volume considered for the calculation of the RDFs is defined by the azimuthal angle θ, satisfying the condition $0 \leq \theta \leq 30°$, as shown in the picture inserted in Figure 3. The decomposition of Pt-OW/HW RDFs into angle-solved RDFs is given in Figure 3b.

The cisPt-W Pt−OW decomposition shows a first intense maximum for the Pt−OW RDF at 3.6 Å, which integrates to *n* ∼ 3 water molecules, and a second peak at 6.4 Å (Figure 3b, left). In the case of Lopes et al.'s potential, there is also a defined peak at 3.6 Å whose integration gives 3 water molecules (Figure 3b, right), although this is due to a higher value of the minimum of the peak, which suggests a less defined axial hydration. This is confirmed by the RDF at larger r_{Pt-OW} where

dx.doi.org/10.1021/ct400433c | J. Chem. Theory Comput. XXXX, XXX, XXX−XXX

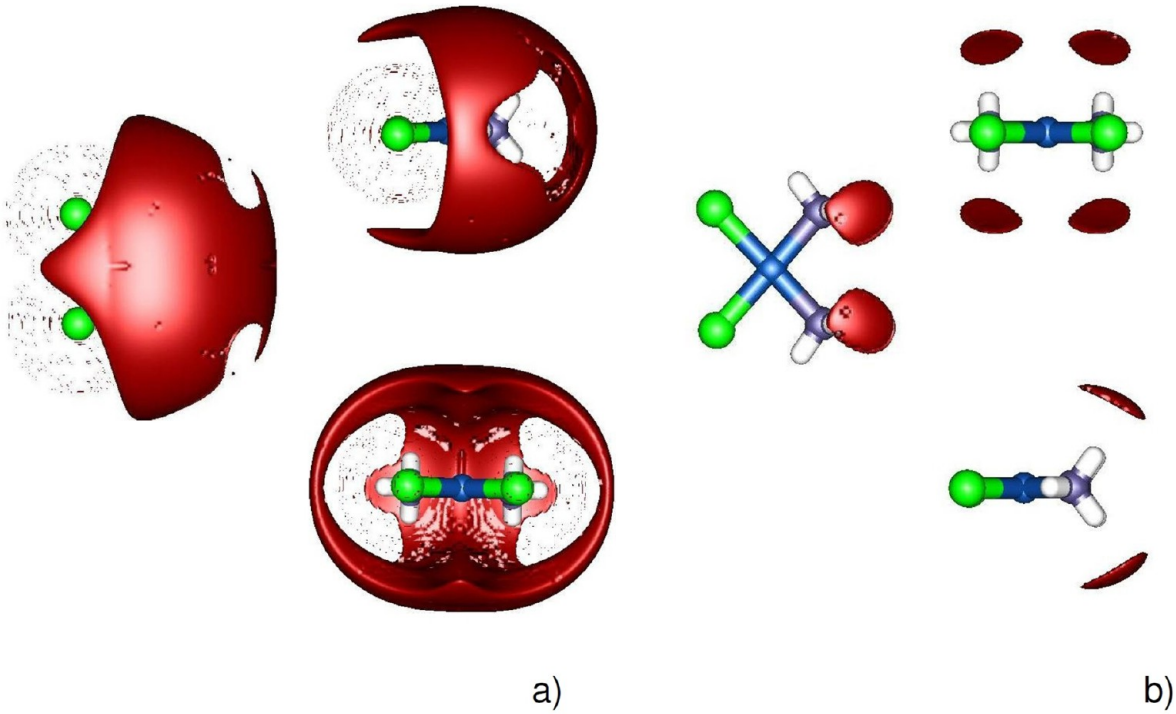

Figure 2. Isopotential surfaces (E_{iso} = −8.5 kcal mol^{-1}) for (a) cisPt-W potential and (b) Lopes at al.'s LJ potential.

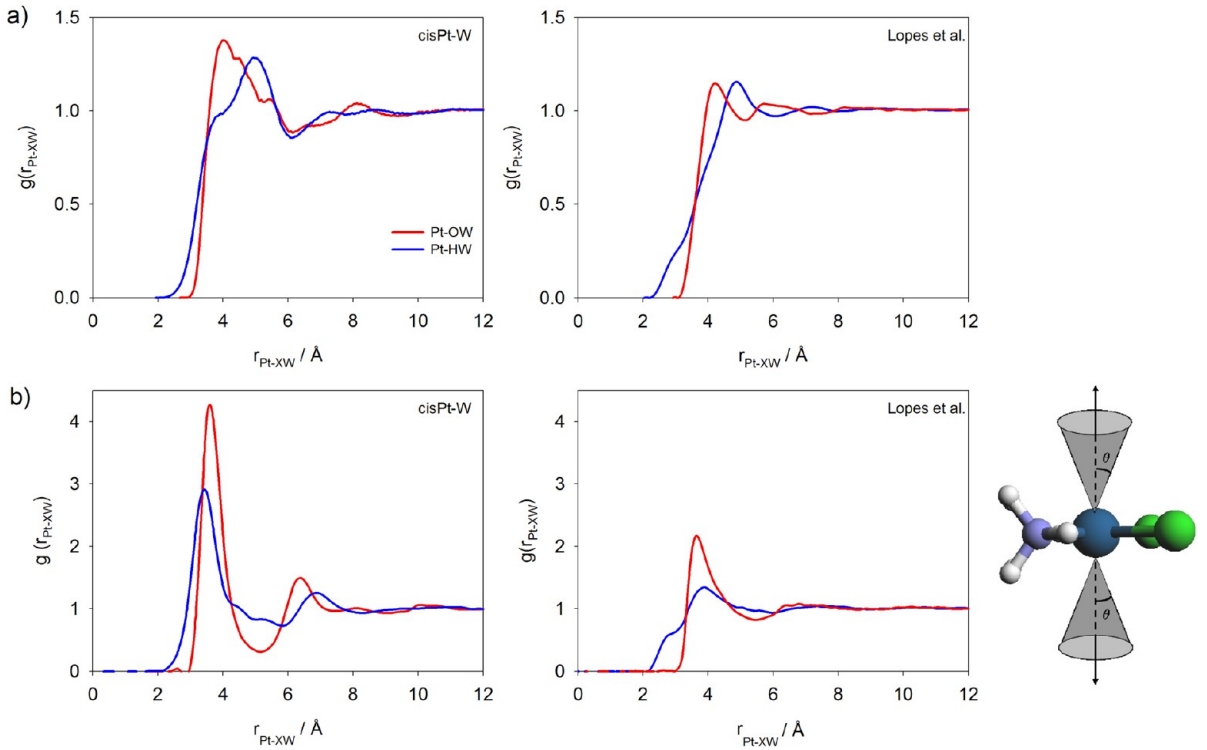

Figure 3. Pt-OW(red) and Pt-HW(blue) RDFs obtained with the cisPt-W potential (left) and Lopes et al.'s potential (right): (a) global RDF; (b) angle-solved RDFs for the axial region defined by the azimuthal angle 0° < θ < 30°.

no well solved second maximum is found. The RDFs comparison shows that the cisPt-W potential has a more structuring effect on this region. However, the analysis of both the global and the partial Pt−OW RDF indicates that the characteristic water molecules, called *meso-shell*, found in the axial region for the Pd(II) hydrate, which exhibits physicochemical properties in between the first and second hydration shells,[24,27,30,51] are not present in the cisplatin case (Figure 3b). Neither of the previous works[20,21] on cisplatin find the *meso-shell* structure. That is, no water molecules are found in the closest axial environment of the Pt(II) ion. It must be underlined that average water distances to the central cation are longer than 3.5 Å, so that condensed medium properties of

dx.doi.org/10.1021/ct400433c | J. Chem. Theory Comput. XXXX, XXX, XXX−XXX

Table 3. Position of the First Peak of the RDF Calculated in This Work and in the Previous Classical and *Ab Initio* MD and MC Simulations

	this work		Fu et al.[21]		Lopes et al.[20]		Lau et al.[17]		Mori et al.[22]	
i–*j*	first maximum (Å)	*n*	first maximum (Å)	*n*	first maximum (Å)	*n*	first maximum (Å)	*n*	first maximum (Å)	*n*
Pt–OW	3.98	28.0	4.2	12.4	4.45	18.9	4.14[a]		4.02	
Pt–HW	4.93	57.1	4.8	22.2	4.95	24.5	4.87[a]			
Cl–OW	3.52	12.6	3.6	10.0	3.65	6.8	3.23	2.9		
Cl–HW	3.28	37.7	2.6	1.2	2.65	0.9	2.25	1.7	2.45	3.6
N–OW	3.13	7.2	2.8	4.1	2.95	3.6	2.95	2.9		
N–HW	3.58	17.3	3.4[b]	12.4[b]						

[a]Values taken from Figure S3 of the reference. [b]Not reported in the original article, obtained by MD simulations in this work.

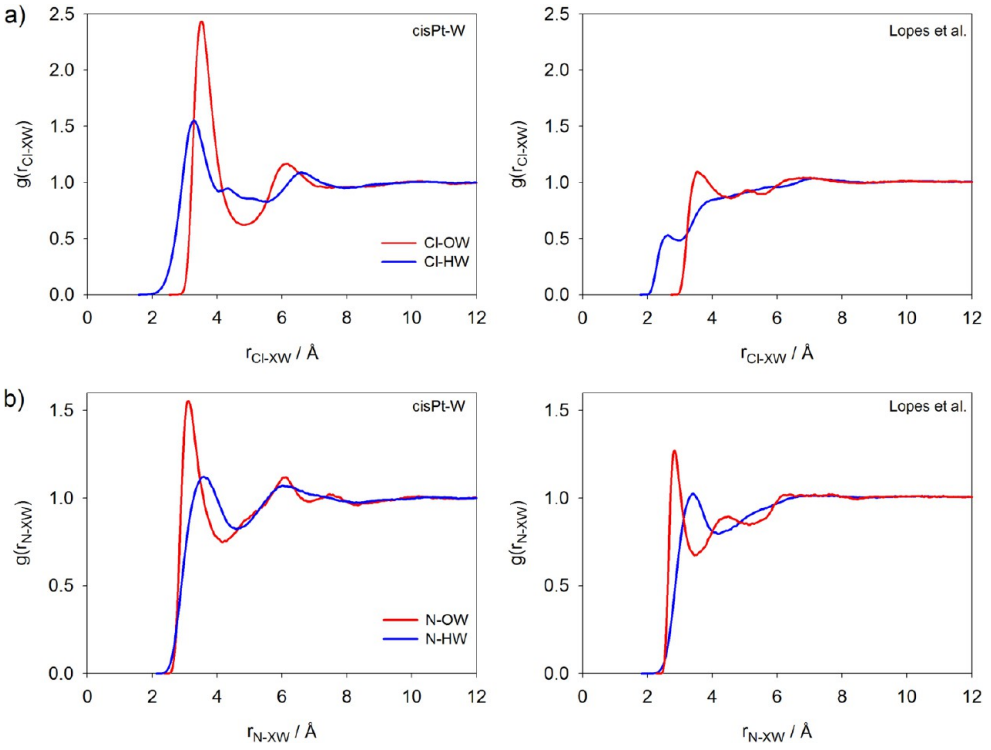

Figure 4. Chlorine–water (a) and nitrogen–water (b) RDFs calculated with the cisPt-W potential (left) and Lopes et al.'s potential (right).

liquid water are mainly responsible of the axial water presence together with the square-planar topology of the solute.

The cisPt-W angle-solved Pt-HW RDF (Figure 3b, left) displays a first maximum at 3.5 Å (n = 3.5), which is responsible of the hump in the first peak of the global RDF, and a second defined peak at 6.9 Å. A wide peak centered at 3.9 Å (n = 7.4) is obtained with Lopes et al.'s potential (Figure 3b, right). From the relative Pt–OW and Pt–HW peak positions and shapes, it seems that in the axial region water molecules weakly bonded ($r_{Pt\text{-}OW} \sim 3.5$ Å) tend to keep parallel to the cisplatin molecular plane during the simulation with the cisPt-W potential. For Lopes et al.'s potential simulation, there is a slightly more pronounced anionic-type hydration tendency as suggested by the presence of a shoulder between 2 and 3 Å in the Pt-HW RDF, which is absent in the Pt-OW case, although the statistical weight of this shoulder is really small. Recently, Bergés et al.[16] have examined the axial water–cisplatin interaction by quantum-mechanical computations. They find a much more defined "inverse hydration" (or anionic-type hydration) than that found in the MD simulations. This apparent discrepancy seems to be solved when one considers the solvent–solvent interactions and the thermal energy, which are incorporated by statistical simulations. Both factors must cause a relaxation of the quantum-mechanical structure, which supports the anionic orientation. The axial approaching water–cisplatin curves, which have been used in the cisPt-W potential, are shown in Figure S5 (SI). The predicted minimum found by Bergés at al. appears in our curves.

RDFs centered on ligand atoms are shown in Figure 4. The Cl-OW RDF obtained with the cisPt-W potential (Figure 4a, left) has two maxima centered at 3.5 (n = 12) and 6.0 Å. These values compare well with the RDF of the previous classical MD simulation,[21] which gives maxima at 3.6 (n = 10.0) and 6.2 Å. However, rather different results are observed in the classical MC[20] and *ab initio* MD simulations;[17] in particular, their coordination numbers much lower, $n \sim 7$ and 3, respectively. Results might be biassed by cell dimensions in the *ab initio* MD case. The Cl-HW RDF (Figure 4a left) presents two maxima at 3.4 and 6.7 Å and have a markedly different shape with respect to the RDF obtained with Lopes et al.'s potential (Figure 4a, right), where a small peak at 2.6 Å appears. The same small peak at $r_{Cl-HW} < 2.65$ Å is also present in Lopes et al. MC simulation.[20] Mori et al.'s FMO-MD results present this shoulder centered even at a shorter distance, 2.45 Å.[22] Once

dx.doi.org/10.1021/ct400433c | J. Chem. Theory Comput. XXXX, XXX, XXX–XXX

more, it is seen that Lopes et al.'s potential builds a much less defined hydration structure around chloride anions.

The angular decomposition of these two global Cl−water RDFs were obtained by considering the volume defined by $0 \leq \theta \leq 90°$ as shown in the sketch of Figure S3 (SI). The presence of two different peaks separated by 1.3 Å in the decomposed Cl-HW RDF obtained with Lopes et al.'s potential suggests that the hydrogen bond involving the chlorine atom tend to be more linear than in the cisPt-W potential case. The origin of this different behavior is likely due both to the different cisplatin−water potential and to the water model used. On one side, the first peaks are more defined for the cisPt-W potential (Figure S3a). On the other side, the smaller intermolecular water−water interaction of the TIP3P model with respect to the SPC/E favors the greater trend of Lopes et al.'s simulation toward an anionic orientation of the water molecules in the chlorine vicinity.

The N−OW RDF presents a first maximum at 3.1 Å ($n \sim 7$)(Figure 4b, left). This maximum is shifted with respect to the previous classical[21,20] and *ab initio* MD simulations,[17] as can be seen in Table 3, and the coordination number is also larger. The N−HW RDF presents a first peak centered at 3.6 Å ($n \sim 17$, Table 3). The simulation with Lopes et al.'s potential produces a similar distribution: a first maximum at 3.4 Å with a peak integration of ∼13 (Figure 4b, right). The angle-solved RDFs are quite similar in shape for the two potentials (Figure S3b, SI) and differ by a small displacement of the peaks and their corresponding running coordination numbers. (Table 4).

Table 4. Maxima Positions of the Angle-Solved RDFs Calculated in This Work with the cisPt-W and Lopes et al.'s Potentials (Figures 3b and S3)[a]

	cisPt-W potential		Lopes et al.'s potential	
i−*j*	first maximum (Å)	*n*	first maximum (Å)	*n*
Pt−OW	3.51	2.9	3.63	2.9
Pt−HW	3.51	7.3	3.88	7.4
Cl−OW	3.44	8.4	3.63	8.9
Cl−HW	3.29	23.4	2.59(3.89)	1.1(23.8)
N−OW	3.14	5.0	2.85	4.1
N−HW	3.59	13.8	3.37	12.6

[a]In parentheses the values for the second maximum are reported for the RDF obtained with the Lopes et al.'s potential (Figure S3a, dashed line).

Water molecules in the equatorial plane can be analyzed by the angular decomposition of the global Pt−OW and Pt−HW RDFs, as defined by the angle θ formed by the vector bisecting the X−Pt−X angle in the molecular plane and the Pt−OW vector (under the condition $0 \leq \theta \leq 30°$) as shown in Figure 5. In the chloride region (Figure 5a), a single oxygen peak centered at 4.5 Å ($n \sim 5$, Table 5) and a wide peak in the Pt−HW RDF exhibiting a hump ∼0.7 Å before the maximum are observed. This seems to indicate that water molecules of the region bisecting the Cl−Pt−Cl angle are partially oriented following a hydrogen-bond arrangement. A snapshot of the MD simulation with a water molecule in a representative orientation is shown in Figure S4a (SI). The RDFs obtained by Lopes et al.'s potential show much lesser intense and broader maxima in the chlorine region, the hydrogen peak being split in a greater extent than in the cisPt-W case. In the ammonia region (Figure 5b), the most striking difference between the two simulations is the intensity of the decomposed Pt−OW RDF, which indicates a higher average number of water molecules in the region between the nitrogen atoms for the simulation with the cisPt-W potential.

3.3. Hydration of Cisplatin: Spatial Distribution Functions. Spatial distribution functions for water oxygen and hydrogen atoms represented with the same cutoff values give an overall 3D-view of the hydration structure obtained by the two potentials (Figure 6). Iso-surfaces have been built for a value 2.5 times that of the average solvent density. Wider oxygen and hydrogen distributions are observed for the cisPt-W-potential simulation. This agrees with the higher hydration number determined for the closest complex environment (Table 3) and appears as a consequence of the general topology exhibited by the potential map plotted in Figure 2. Furthermore, SDF shapes are also rather different, as expected from the different shape of the global and partial RDFs. In the axial region, the SDF is nearly absent for the simulation carried out with Lopes et al.'s potential (Figure 6b, middle). From the two side views, it is seen that the oxygen SDF forms a narrow lobe bisecting the Cl−Pt−Cl angle (Figure 6b, left), as already observed by Fu et al. in their MD simulations.[21] For the cisPt-W potential, the hydrogen bond formed by the chlorine and the water hydrogen is much more defined than for that of Lopes et al.'s, as a consequence, higher values are observed in the RDFs (Figure 5a, left), although, interestingly, it is in the intermediate Cl region where H atom population is higher. Figure S3a (SI) plots a representative structure taken from a snapshot where this arrangement is shown. The region around ammonia groups also shows different features: whereas water oxygen atoms are quite evenly distributed around the ammonia ligands in the cisPt-W case (Figure 6a, left), Lopes et al.'s SDF is strongly located in the vicinity of the hydrogen atoms (Figure 6b, left). It is interesting to note that such distributions roughly correspond to the regions where the two potentials reach their most negative values (Figures 2 and S4b (SI)).

3.4. Operational Definition of the Hydration Number on a Multisite Solute. After this thorough analysis of the relevant global and angle-solved RDFs that have scanned the different solvent regions around the Pt(II) complex, it is possible to undertake a general view of the hydration shell around the complex. The usual way of answering this issue is based on the analysis of the global RDF of the central metal cation (Figure 3 and Table 3). Nevertheless, the intrinsic nonradial topology of the complex and the rather different nature of the surrounding ligands preclude to extract a proper answer from this analysis. The examination of the angle-solved and the global RDFs centered on the relevant ligand atoms give additional information about the local hydration, but the overlap regions makes difficult a unique interpretation of the global hydration. To get an alternative solution to this problem, we have collected along the MD trajectory the number of water molecules that are inside the region defined by the spheres centered on the Pt, N, and Cl atoms of the complex. These sphere radii are equal to the X-O distance of the first minimum in the corresponding angle-solved X−O RDFs (cf. Figures 3b and S3). By adopting this criterion, we are defining a molecular volume that corresponds to the metal complex and its first hydration shell as plotted in Figure 7 (blue surfaces). The average number of water molecules is 27.4 and 22.0 for the MD simulations using the cisPt-W and Lopes et al.'s potential, respectively. For the sake of comparison, the spheres centered on Pt with a sphere radius equals to the Pt-OW distance of the first minimum in the corresponding RDFs (cf. Figure 3a) are

dx.doi.org/10.1021/ct400433c | J. Chem. Theory Comput. XXXX, XXX, XXX−XXX

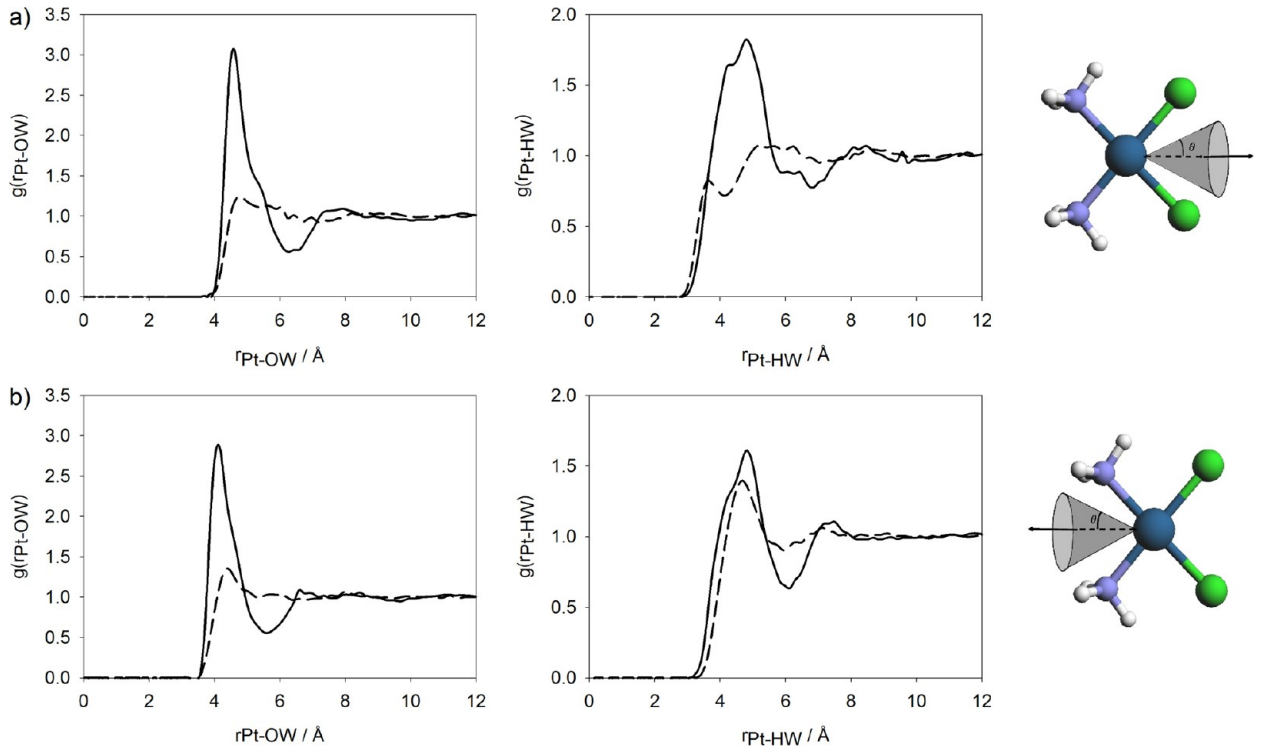

Figure 5. Angle-solved Pt-OW and Pt-HW RDFs for (a) Cl-region; (b) NH_3-region. The RDF is calculated for the volume defined by $0° \leq \theta \leq 30°$. The RDF is calculated with the cisPt-W potential (solid line) or Lopes et al.'s potential (dashed lines).

Table 5. Maxima Positions of the Angle-Solved RDFs Calculated with the Indicated Intermolecular Potentials (Figure 5)

	cisPt-W potential		Lopes et al.'s potential	
i–*j*	first maximum (Å)	*n*	first maximum (Å)	*n*
	Chloride Side			
Pt–OW	4.51	4.7	4.82	4.8
Pt–HW	4.86	12.0	3.73	1.4
	Ammonia Side			
Pt–OW	4.13	3.3	4.36	2.0
Pt–HW	4.86	7.3	4.67	6.6

also plotted in Figure 7 (yellow point grid). As already given in Table 3, due to the difference in the shape of both Pt-OW RDFs, their running integration numbers differ a lot. By using a multicenter definition, the hydration number becomes much more similar. The overlapping among the spheres centered on different atoms precludes a complete ascription of each water molecule to only one of the interlocking spheres, that is, to a given center and by extension to a given ligand, in the case of the cisPt-W simulation, a 55% of the first-shell water molecules can be ascribed to a particular region, whereas a 35% belongs to regions where two spheres mutually overlap. In the case of Lopes et al.'s simulation, the values are: 42% (water molecules only in one sphere) and 39% (water molecules in 2-spheres overlaping regions). It must be pointed out that the current criterion leads to a difference in the first hydration number estimation between both simulations of 5 water molecules (27 for cisPt-W vs. 22 for Lopes et al.'s potential), whereas this difference increases up to 16 (28 vs. 12) when the single Pt center RDF was employed.

A final remark about the meaning and intrinsic nature of the multicenter volume defined in Figure 7 is worth being made. At first sight, this figure might look like the molecular volume of the solute, i.e. the cisplatin. However, it has been built on the basis of radii matching the first minima of Pt–OW, N–OW, and Cl–OW distribution functions. This means that the region enclosed by this multicenter surface defines the molecular form of the hydrated Pt(II) complex in solution, through the inclusion of the statistical solvent distribution.

3.5. Potential Behaviors: Examining Their Differences.

Regarding the behavior of the intermolecular cisPt-W potential here developed, there are two methodological points which deserve special attention:

(i) What is the impact of the continuum model inclusion in the intermolecular potential?

(ii) What is the impact of the addition of r^{-4} and r^{-8} terms to the usual Lennard-Jones functional form?

Point i can be understood by means of a set of interacting curves corresponding to the axial approach of a water molecule to the cisplatin complex (Figure 8). In one case, a stabilizing approach is defined by the *antiparallel* arrangement of the molecular dipoles, whereas in the second case, the approaching is repulsive as mutual dipole orientation is *parallel*. The classical curves derive from the dipole–dipole electrostatic interaction computed with the dipoles of the fragments coming from either the gas phase or the PCM polarized wave function of the cisplatin and the water molecule (solid lines) are plotted in Figure 8. The quantum mechanical interaction energy (dashed lines) predicted by the computation of the two molecules isolated (gas phase) or both of them polarized by the dielectric continuum, that is, U_{AB} defined by eq 2, is also shown in the figure. Analysis of curves behavior indicates that continuum solvent effects give an additional attracting interaction for the antiparallel orientation, since polarization effects have increased the individual molecular dipole moments of both interacting

dx.doi.org/10.1021/ct400433c | J. Chem. Theory Comput. XXXX, XXX, XXX–XXX

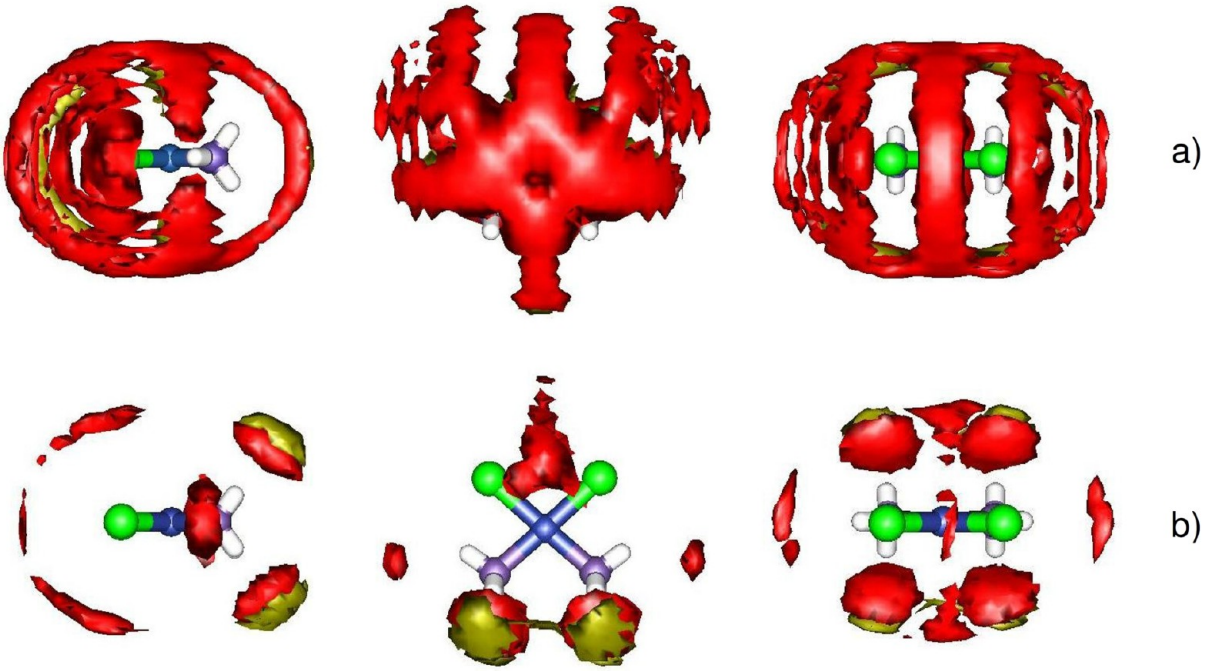

Figure 6. SDF for oxygen (red) and hydrogen (yellow) calculated using the (a) cisPt-W and (b) Lopes et al.'s potentials (iso-surface value = 2.5 times average solvent density).

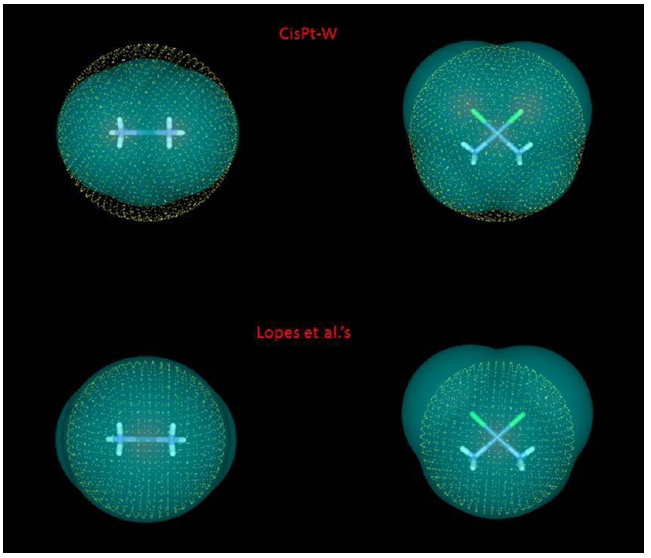

Figure 7. Equatorial and axial views of the cisplatin and the surface involving its first hydration shell (blue surfaces). Dotted yellow spheres are centered on the Pt(II) ion and their radii corresponds to the minimum of the first Pt−OW RDF peak.

molecules. For the same reason, when the orientation is parallel, it becomes more repulsive for the solvent polarized case. It is interesting to check that quantum mechanical results follow the same trend. Even more, the classical curves almost match the quantum mechanical for distances as short as 5 Å for the attractive orientation. Nonelectrostatic effects become important at shorter intermolecular distances as mutual wave function polarization moderate the interaction for both cases, the repulsive and the attractive ones. As a general conclusion, the use of solvent-polarized wave function to build our interaction potential yields to a more attractive potential compared to the gas phase case.

Point ii is joined to the change in the structural results due to the change of the functional form of the interaction potential from a classical Lennard-Jones expression to a four-term r^{-n} expression. The comparison between RDFs of the MD simulations carried out with the cisPt-W and cisPt-W/LJ potentials is provided in Figure 9. The only difference between both potentials is that the functional form of cisPt-W contains two additional terms, r^{-4} and r^{-8}, but both of them have been fitted with respect to the structure set of the same energy surface (see Section 3.1). It is shown in the figure that pair distributions are mainly different at short distances what means these terms affect to the first hydration shell water molecules. Unexpectedly, although the position of the main peaks are quite similar for the two simulations, their intensities are not. It is worth mentioning that cisPt-W/LJ RDFs resembles the shape of those of Lopes et al.'s potential (cf. Figures 3a, right, and 4, right, vs Figure 9), stressing the relevance of the functional form chosen when fitting a given energy surface.

The analysis of the two previous points supplies pieces of information that allows the understanding of the different behavior of the cisplatin−water potential here developed and that previous developed by Lopes et al.[20] The more attracting nature of cisPt-W potential comes from the inclusion of solvent polarized wave function of interacting particles in the potential building and from the full BSSE correction included by Lopes et al. in the ab initio interaction energies considered. A second factor affecting the hydration structure is the inclusion of the r^{-4} and r^{-8} terms in our cisPt-W potential, which, globally, leads to a more structured hydration by extending the attractive region around the solute.

4. CONCLUDING REMARKS

A new classical cisplatin−water interaction potential has been proposed in this work by fitting about 4000 *ab initio* interaction energies calculated at the MP2 level. This new potential building differs from previous works in the fact that solvent

dx.doi.org/10.1021/ct400433c | J. Chem. Theory Comput. XXXX, XXX, XXX−XXX

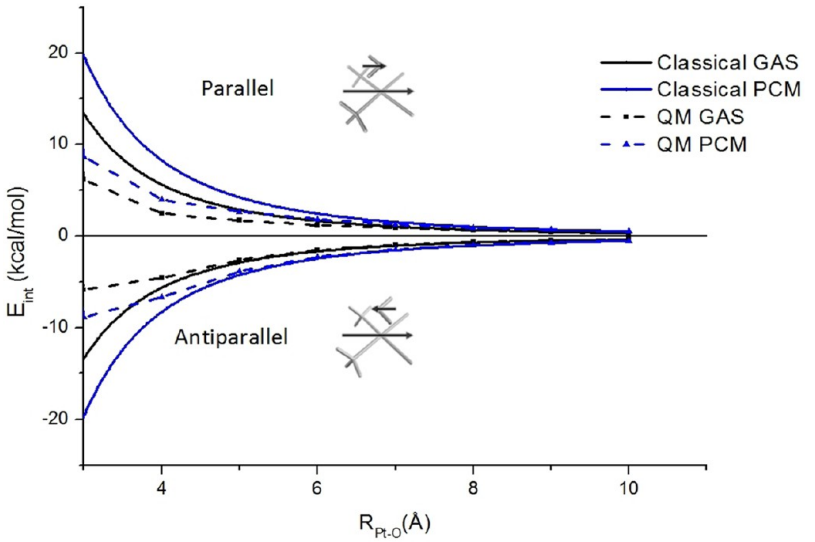

Figure 8. Cisplatin−water interaction curves for parallel and antiparallel dipole moment arrangements estimated by analytical classical electrostatics (solid line) or quantum−mechanical computations (dashed line) using either the gas phase or solvent PCM polarized conditions.

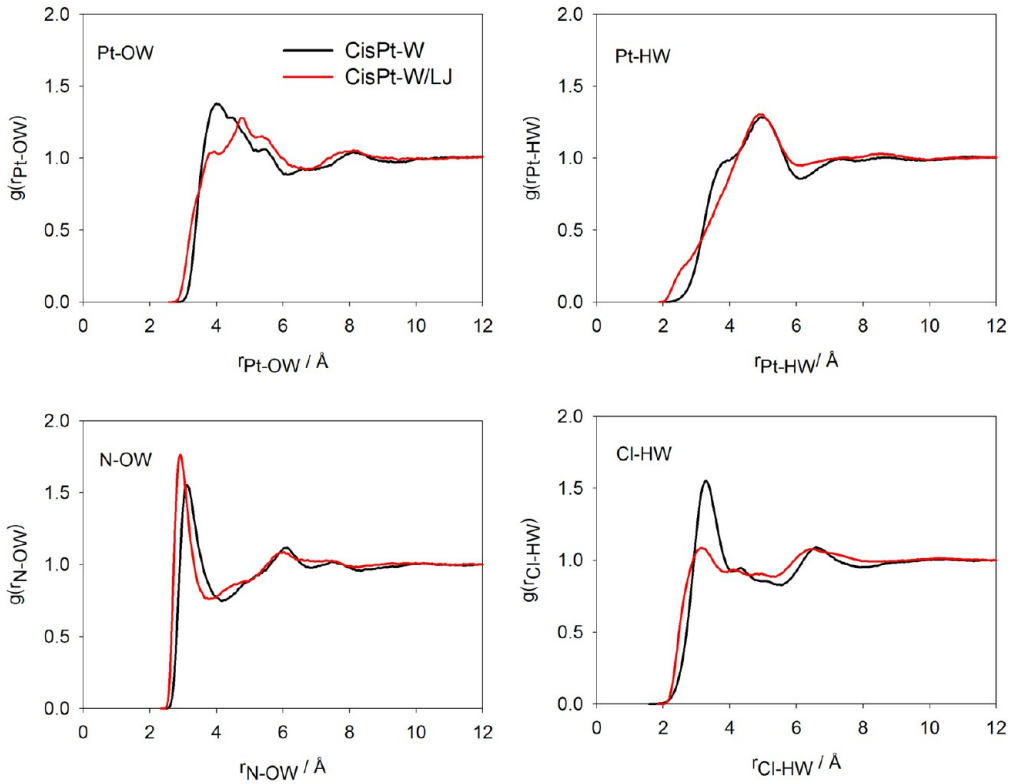

Figure 9. Representative RDFs of the cisplatin in water corresponding to MD simulations carried out using the cisPt-W and the cisPt-W/LJ potentials.

effects on the dimer interaction (cisplatin−water) have been taken into account by a polarizable continuum model that provides *average* many-body effects. In some way, interaction potentials built with this methodology bring the solute−solvent interaction during the simulation to the same foot as the water−water one: most of the nonpolarizable solvent models reproducing bulk properties are based on "effective" potentials where condensed medium polarization effects are implicitly taken into account, for example, by increasing the gas phase dipole moment. The new cisPt-W functional form (eq 4) gives additional flexibility to the conventional 12−6 form and better reproduces the *ab initio* interaction energies, especially for the most attractive points. The Lennard-Jones potential form is physically sounding (i.e., the potential energy systematically tends to infinite at short distance) and is practical, since no modification of computer simulation codes is needed. However, it has only two parameters for each atom type, which, in the previous works,[20] were fitted with a relatively small number of *ab initio* interaction energies.[20] The cisPt-W potential, due to its higher degree of flexibility, reproduces with higher accuracy the

dx.doi.org/10.1021/ct400433c | J. Chem. Theory Comput. XXXX, XXX, XXX−XXX

complex molecular shape defined by the cisplatin−water interaction. This is particularly true for the most attractive interaction regions. It is worth pointing out that there is an implicit parallelism among the number of structures considered for the fitting, the diversity of arrangements and the number of r^{-n} terms employed in the fit. The intermolecular LJ potential is able to fit reasonably well a reduced number of structures, providing local attracting regions around the ligand complex. However when this functional form is employed to fit a larger amount of structures and interaction energies, the ability to mimic the details not only within the most attractive regions, (or *in situm* in the classical super molecule terminology[52]) but also in the medium-attractive regions (*ad situm*) and the nonattractive ones (*extra situm*) is limited. When adding the two additional r^{-n} powers to the potential function, its flexibility increases and a widespread interaction region is properly described.

When a comparative analysis of the trajectories is made, significant differences in the hydration structure of cisplatin with respect to previous classical and *ab initio* molecular simulations are found: (a) Following the RDF based on the central atom of the complex, now a much higher hydration number is obtained with the cisPt-W potential. This reflects that significant attractive regions are spread around the ligands. (b) The RDF decomposition shows that three axial water molecules are obtained in both simulations, but the peak shape and intensity are very different (Figure 3 and 4). (c) The Cl−HW RDF analysis shows that water has a different average orientation in our model (Figure 4) while the N−OW/HW RDFs are quite similar (Figure 4) . These results are also evident from the SDFs (Figure 6). The best adapted definition of first hydration shell around this square−planar complex is achieved when a multicenter-based surface defined by the overlapping of spheres centered on the main atoms of the complex is built. Their sphere radii are taken from the corresponding minima in their angle-solved X−OW RDF. Thus, an estimation of 27 water molecules in the first hydration shell is obtained.

The good behavior of the method here established must facilitate further research of related intermolecular potentials based on first-principles. Thus, new classical MD simulations can undertake the statistical description of the cisplatin hydrolysis processes in successive substitution of chloride ligands by water molecules, as well as the statistical description of other Pt(II) complexes where the ammine ligands are replaced by other N-coordinating carrier groups.

■ ASSOCIATED CONTENT

Ⓢ Supporting Information

Interaction energy curves of cisplatin−water approaching computed with different basis sets and with or without BSSE counterpoise correction. Plot of the fitted vs *ab initio* interaction energies for the cisPt-W and cisPt-W/LJ potentials. Angle-solved C−OW, Cl−HW, N−OW, and N−HW RDFs. Snapshots from MD simulations. Curves of interaction potential along the axial and the equatorial regions. Fitted coefficients for the cisPt-W/LJ potential. This material is available free of charge via the Internet at http://pubs.acs.org.

■ AUTHOR INFORMATION

Corresponding Author

*Phone: +34 954557175. Fax: +34 954557174. E-mail: sanchez@us.es.

Notes

The authors declare no competing financial interest.

■ ACKNOWLEDGMENTS

The Spanish DGI of the Ministerio de Economia y Competitividad is acknowledged for financial support (CTQ2011-25932) and "Programa de Movilidad de jóvenes doctores"(SB2009-0081). A.M. thanks the Italian Ministry of Education, University and Research (MIUR) (project PRIN 2010−2011 NANO Molecular Technologies for Drug Delivery-NANOMED).

■ REFERENCES

(1) Kelland, L. *Nat. Rev. Cancer* **2007**, *7*, 573−584.
(2) Jamieson, E. R.; Lippard, S. J. *Chem. Rev.* **1999**, *99*, 2467−2498.
(3) Perez, R. P. *Eur. J. Cancer* **1998**, *34*, 1535−1544.
(4) Reedijk, J. *Chem. Rev.* **1999**, *99*, 2499−2510.
(5) Robertazzi, A.; Platts, J. A. *Chem.—Eur. J.* **2006**, *12*, 5747−5756.
(6) Cerón-Carrasco, J. P.; Jacquemin, D.; Cauët, E. *Phys. Chem. Chem. Phys.* **2012**, *14*, 12457−12464.
(7) Teletchea, S.; Skauge, T.; Sletten, E.; Kozelka, J. *Chem.—Eur. J.* **2009**, *15*, 12320−12337.
(8) Zimmermann, T.; Leszczynski, J.; Burda, J. V. *J. Mol. Model.* **2011**, *17*, 2385−2393.
(9) Burda, J. V.; Zeizinger, M.; Leszczynski, J. *J. Chem. Phys.* **2004**, *120*, 1253−1262.
(10) Deubel, D. V. 2004, *126*, 5999-6004.
(11) Robertazzi, A.; Platts, J. A. *J. Comput. Chem.* **2004**, *25*, 1060−1067.
(12) Deubel, D. V. *J. Am. Chem. Soc.* **2006**, *128*, 1654−1663.
(13) Pavelka, M.; Lucas, M. F. A.; Russo, N. *Chem.—Eur. J.* **2007**, *13*, 10108−10116.
(14) Lucas, M. F. A.; Pavelka, M.; Alberto, M. E.; Russo, N. *J. Phys. Chem. B* **2009**, *113*, 831−838.
(15) Alberto, M. E.; Lucas, M. F. A.; Pavelka, M.; Russo, N. *J. Phys. Chem. B* **2009**, *113*, 14473−14479.
(16) Bergés, J.; Fourré; Pilmé, J.; Kozelka, J. *Inorg. Chem.* **2013**, *52*, 1217−1227.
(17) Lau, J. K.-C.; Ensing, B. *Phys. Chem. Chem. Phys.* **2010**, *12*, 10348−10355.
(18) Melchior, A.; Sanchez Marcos, E.; Pappalardo, R. R.; Martinez, J. M. *Theor. Chem. Acc.* **2011**, *128*, 627−638.
(19) Paschoal, D.; Marcial, B. L.; Lopes, J. F.; De Almeida, W. B.; Dos Santos, H. F. *J. Comput. Chem.* **2012**, *33*, 2292−2302.
(20) Lopes, J. F.; de A. Menezes, V. S.; Duarte, H. A.; Rocha, W. R.; De Almeida, W. B.; Dos Santos, H. F. *J. Phys. Chem. B* **2006**, *110*, 12047−12054.
(21) Fu, C.-F.; Tian, S. X. *J. Chem. Phys.* **2010**, *132*, 174507.
(22) Mori, H.; Hirayama, N.; Komeiji, Y.; Mochizuki, Y. *Comput. Theor. Chem.* **2012**, *986*, 30−34.
(23) Ayala, R.; Sánchez Marcos, E.; Diaz-Moreno, S.; Sole, V. A.; Muñoz Paez, A. *J. Phys. Chem. B* **2001**, *105*, 7588−7593.
(24) Naidoo, K. J.; Klatt, G.; Koch, K. R.; Robinson, D. J. *Inorg. Chem.* **2002**, *41*, 1845−1849.
(25) Truflandier, L. A.; Autschbach, J. *J. Am. Chem. Soc.* **2010**, *132*, 3472.
(26) Truflandier, L. A.; Sutter, K.; Autschbach, J. *Inorg. Chem.* **2011**, *50*, 1723−1732.
(27) Torrico, F.; Pappalardo, R. R.; Sanchez Marcos, E.; Martinez, J. M. *Theor. Chem. Acc.* **2006**, *115*, 196−203.
(28) Beret, E. C.; Pappalardo, R. R.; Marx, D.; Sanchez Marcos, E. *ChemPhysChem* **2009**, *10*, 1044−1052.
(29) Hofer, T. S.; Randolf, B. R.; Rode, B. M.; Persson, I. *Dalton Trans.* **2009**, 1512−1515.
(30) Martinez, J. M.; Torrico, F.; Pappalardo, R. R.; Sanchez Marcos, E. *J. Phys. Chem. B* **2004**, *108*, 15851−15855.
(31) Beret, E. C.; Provost, K.; Mueller, D.; Sanchez Marcos, E. *J. Phys. Chem. B* **2009**, *113*, 12343−12352.

(32) Provost, K.; Beret, E. C.; Bouvet-Mueller, D.; Michalowicz, A.; Sanchez Marcos, E. *J. Chem. Phys.* **2013**, *138*, 084303−1−084303−10.
(33) Floris, F. M.; Martinez, J. M.; Tomasi, J. *J. Chem. Phys.* **2002**, *116*, 5448−5459.
(34) Floris, F. M.; Martinez, J. M.; Tomasi, J. *J. Chem. Phys.* **2002**, *116*, 5460−5470.
(35) Kozelka, J.; Bergés, J.; Attias, R.; Fraitag, J. *Angew. Chem., Int. Ed., Engl.* **2000**, *39*, 198−201.
(36) Andrae, D.; Haussermann, U.; Dolg, M.; Stoll, H.; Preuss, H. *Theor. Chim. Acta* **1990**, *77*, 123−141.
(37) Berendsen, H. J. C.; Grigera, J. R.; Straatsma, T. P. *J. Phys. Chem.* **1987**, *91*, 6269−6271.
(38) Tomasi, J.; Mennucci, B.; Cami, R. *Chem. Rev.* **2005**, *105*, 2999−3093.
(39) Floris, F.; Persico, M.; Tani, A.; Tomasi, J. *Chem. Phys. Lett.* **1992**, *199*, 518−524.
(40) Boys, S. F.; Bernardi, F. *Mol. Phys.* **1970**, *19*, 553−566.
(41) Jensen, F. *J. Chem. Theory Comp.* **2010**, *6*, 100−106.
(42) Alvarez-Idaboy, J. R.; Galano, A. *Theor. Chem. Acc.* **2010**, *126*, 73−85.
(43) Kim, K. S.; Tarakeshwar, P.; Lee, J. Y. *Chem. Rev.* **2000**, *100*, 4145−4185.
(44) Cook, D. B.; Sordo, T.; Sordo, J. A. *J. Chem. Soc. Chem. Comm.* **1990**, 185−186.
(45) Frisch, M. J.; Trucks, G. W.; Schlegel, H. B.; Scuseria, G. E.; Robb, M. A.; Cheeseman, J. R.; Scalmani, G.; Barone, V.; Mennucci, B.; Petersson, G. A.; Nakatsuji, H.; Caricato, M.; Li, X.; Hratchian, H. P.; Izmaylov, A. F.; Bloino, J.; Zheng, G.; Sonnenberg, J. L.; Hada, M.; Ehara, M.; Toyota, K.; Fukuda, R.; Hasegawa, J.; Ishida, M.; Nakajima, T.; Honda, Y.; Kitao, O.; Nakai, H.; Vreven, T.; Montgomery, J. A., Jr.; Peralta, J. E.; Ogliaro, F.; Bearpark, M.; Heyd, J. J.; Brothers, E.; Kudin, K. N.; Staroverov, V. N.; Kobayashi, R.; Normand, J.; Raghavachari, K.; Rendell, A.; Burant, J. C.; Iyengar, S. S.; Tomasi, J.; Cossi, M.; Rega, N.; Millam, J. M.; Klene, M.; Knox, J. E.; Cross, J. B.; Bakken, V.; Adamo, C.; Jaramillo, J.; Gomperts, R.; Stratmann, R. E.; Yazyev, O.; Austin, A. J.; Cammi, R.; Pomelli, C.; Ochterski, J. W.; Martin, R. L.; Morokuma, K.; Zakrzewski, V. G.; Voth, G. A.; Salvador, P.; Dannenberg, J. J.; Dapprich, S.; Daniels, A. D.; Farkas, Ã.; Foresman, J. B.; Ortiz, J. V.; Cioslowski, J.; Fox, D. J. *Gaussian 09*, Revision C.01; Gaussian Inc.: Wallingford, CT, 2009.
(46) Besler, B. H.; Merz, K. M.; Kollman, P. A. *J. Comput. Chem.* **1990**, *11*, 431−439.
(47) Smith, W.; Yong, C. W.; Rodger, P. M. *Mol. Simul.* **2002**, *28*, 385−471.
(48) Frenkel, D.; Smit, B. *Understanding Molecular Simulation: From Algorithms to Applications*, 2nd ed.; Academic Press: Harcourt, FL, 2002.
(49) Jorgensen, W. L.; Chandrasekhar, J.; Madura, J. D.; Impey, R. W.; Klein, M. L. *J. Chem. Phys.* **1983**, *79*, 926−935.
(50) Beret, E. C.; M., M. J.; Pappalardo, R. R.; Sanchez Marcos, E.; Doltsinis, N. L.; Marx, D. *J. Chem. Theory Comput.* **2008**, *4*, 2108−2121.
(51) Purans, J.; Fourest, B.; Cannes, C.; Sladkov; David, F.; Venault, L.; Lecomte, M. *J. Phys. Chem. B* **2005**, *109*, 11074−11082.
(52) Pullman, A. *Quantum Theory of Chemical Reactions*; Reidel: Dordrecht, Holland, 1981; Vol. *II*, Chapter 1, pp 1−24.